RICE FIELD DETECTION AND MAPPING USING MULTITEMPORAL SENTINEL-1 SYNTHETIC APERTURE RADAR DATA WITH RGB COMPOSITE AND THRESHOLDING APPROACH: A CASE IN THREE DISTRICTS OF CIANJUR, INDONESIA

Muhammad Hayyu Mahabbah (1)(2), Baba Barus (1)(2), Bambang Hendro Trisasongko (1)

[1]Department of Soil Science and Land Resources, IPB University, Meranti road, IPB Darmaga Campus, Bogor 16680, West Java, Indonesia
[2]GITIIA P4W, IPB University, Pajajaran Road, IPB Baranangsiang Campus, Bogor 16124, West Java, Indonesia
Email: mahabbah_53@apps.ipb.ac.id; bbarus@apps.ipb.ac.id; trisasongko@apps.ipb.ac.id

KEYWORDS: Multitemporal SAR data, RGB composite, rice map, Sentinel-1, threshold

ABSTRACT: Sentinel-1 with temporally dense and open access data is a candidate platform suitable for rice monitoring. The objective of this study was to exploit Sentinel-1 C-band Synthetic Aperture Radar (SAR) multitemporal imagery to detect and to map rice cropping areas of Cianjur, Indonesia, through (1) learning the backscattering behavior on rice fields; and (2) generating rice area maps via several thresholding combinations. Layer manipulation (r.series aggregate operation) and RGB false-color composite images were constructed to better visualize the separability of rice areas among other types of land utilization. The result shows the averaged accuracy of about 82% with the highest accuracy of 85.6% using maximum and minimum backscatter coefficient thresholds on VH polarization. We concluded that a simple, straightforward approach could be beneficial for a specific task while minimizing the computational burden for further broad-scale implementation.

1. INTRODUCTION

1.1 Background

Rice has been the main staple food for the majority of people in Indonesia. Estimated rice consumption in this country was around 111.58 kg person^{-1} year^{-1} (Badan Pusat Statistik, 2018). However, rice harvested area and production have declining trends (Panuju et al., 2013; Badan Pusat Statistika, 2019) and remain facing further challenges due to growing population trend, climate change, and unprecedented situations like the Covid-19 outbreak. With such dire complexity, food security continues to be a critical issue that needs to be addressed, and thus monitoring farming activity is important for the authority to develop strategies and policies.

Monitoring systems able to provide information related to rice crops require synoptic and timely data products. In this role, satellite-borne imaging systems can contribute to both time- and cost-effective data acquisition (Kuenzer and Knauer, 2013). To date, they offer a variety of datasets in terms of spatial, radiometric, spectral, and temporal resolution. With frequent cloud cover in a tropical region like Indonesia, Synthetic Aperture Radar (SAR) data outweigh multispectral images as the data source for rice crop monitoring. This is due to its longer wavelength, which is less sensitive to cloud cover, and its independency to solar illumination (Kuenzer and Knauer, 2013; Trisasongko, 2017).

One of the limiting factors for utilizing SAR data for crop monitoring is the lack of data availability (Clauss et al., 2018). Rapid production cycle as shown in rice farming necessitates frequent data acquisition and collection strategies, which are beyond the capability of single-SAR systems and therefore urge the implementation of constellation-type SAR systems. Sentinel-1 constellation – the first satellite of the Copernicus program which was launched in 2014 – attempts to overcome this challenge and it has been gaining popularity as the data source for agricultural monitoring. Global and temporally dense coverage, free, and open access properties are some of the benefits offered to the end-users. This satellite mission generates C-band dual-polarization (VV and VH) data with 3-6 days of temporal resolution and 10 m pixel spacing.

Computational complexity comes to its existence when big satellite data processing is available for public use. Researchers approach the complexity through implementing machine learning models capable to adapt to small sampling data, including random forests and support vector machines. In this article, however, a straightforward, computationally inexpensive strategy using RGB false-color composite and thresholding to detect and rice map is presented. RGB composite technique often used as the first step in SAR data analysis (Refice et al., 2014; Wiesmann et al., 2001), provides a way to distinguish different land cover based on the stability of the SAR signals. Stable signals indicating particular land cover needs to be separated. Thresholding is one of the commonly adopted methods in discrimination problems, including the one implemented in flooded and non-flooded areas, as well as irrigated rice fields (Henry et al., 2006; Wakabayashi et al., 2019). The advantage of thresholding is computational efficiency which makes it beneficial for mapping purposes. The detrimental issues include, however, the determination of threshold value requiring adaptation to environmental conditions depending on the purpose (Stroppiana et al., 2019).

The main purpose of this article is, therefore, two-fold. The first is to investigate the behavior of SAR linear backscatters upon growing rice plants, which establishes the base of the identification of rice fields through a dense stack SAR dataset. In addition, RGB composting strategies are evaluated as an input to the thresholding procedure.

2. STUDY AREA AND DATA

2.1 Study Site

The study was located in the district of Ciranjang, Cianjur, West Java, Indonesia (Figure 1). Paddy fields are mostly managed by the Provincial Agency of Food Crops and Horticulture. The site is situated in a generally flat terrain with a mean elevation of 283 m above sea level. With that topographical benefits, the region is foremost known as an agriculture bread-basket. This area experiences rainfall of around 3700 mm with an average temperature of 29 – 30^{o}C yearly, equipped with existing irrigation networks to assist rice production. Soil type found in the area is generally classified into Inceptisols based on USDA's soil taxonomy system. In-depth rice area detection and mapping were conducted in three districts namely Ciranjang, Haurwangi, and Bojongpicung.

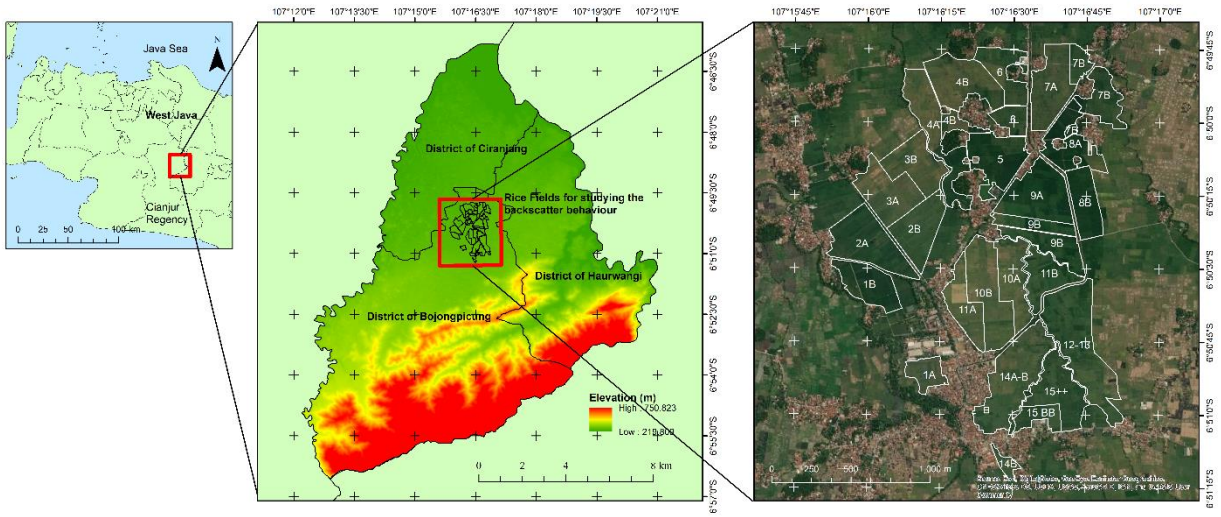

Figure 1 Site map

2.2 Sentinel-1 SAR Data

Each rice field has slightly different rice cultivation scheduling. In the 2019/2020 period, the starting date for the first sowing was in early December 2019 until the last harvesting schedule in late May 2020. For this reason, a total of fifty-two Sentinel-1 images were downloaded from the period between 3 November 2019 and 28 May 2020 (Table 1). These images were downloaded from Copernicus Open Access Hub (https://scihub.copernicus.eu/dhus/#/home).

Table 1 Specifications of Sentinel-1 data

Satellite	Sentinel-1A and Sentinel-1B
Sensor	SAR-C
Product-level	Ground Range Detected (GRD)
Order by	Descending
Date acquisition	3 Nov. 2019 – 27 May 2020
Frequency (GHz)	5.045
Revisit frequency at equator (day)	3 – 6
Pixel spacing	10x10 m
Image mode	Interferometric Wide swath (IW)
Polarization	VV + VH
Incident angle (degree)	29.1° – 46.0°

2.3 Secondary Data

The rice cultivation schedule and the rice map reference were obtained from the Agency, improved with field surveys in January-February 2020. Minor readjusting such as aligning, slippers editing, and reprojection were performed. Rice cultivation schedule contains expected date of sowing, transplanting, and harvesting periods. The rice map reference was verified by a previous study (Munibah et al., 2016)

3. METHODOLOGY

The main steps included Sentinel-1 SAR data pre-processing, Sigma nought (σ^0) value (dB) extraction and descriptive statistics, pixel-wise calculation of maximum, minimum, and difference

from data series (r.series), RGB false-color composite construction and threshold determination, and accuracy assessment using confusion matrix.

3.1 Sentinel-1 Pre-processing

Sentinel-1 data were pre-processed using SNAP (Sentinel Application Platform) open-source software (http://step.esa.int/main/download/) developed by the European Space Agency (ESA). The first step of pre-processing was to apply a precise orbit file. Orbit state vectors provided in SAR metadata are generally inaccurate and can be refined using precise orbit files. Thermal noise removal was then applied to revoke noises from the product. Subsequently, calibration was done to convert digital number values of Sentinel-1 images into backscattering coefficient. Radiometric correction was necessary to represent radar backscatter.

Due to topographical variations, data were then aligned via Range-Doppler Terrain Correction using digital elevation model of the Shuttle Radar Topography Mission (SRTM) 1Sec HGT and were projected onto WGS 1984 Universal Transverse Mercator (UTM) zone 48S. Each polarization was separated to permit independent investigation of different polarization in detecting rice growth. In addition, geographical subsetting was implemented to reduce processing time. Stacking or co-registration was done according to each polarization to allow temporal processing with chronological order.

Multitemporal speckle filter was then applied employing 7x7 Lee Sigma to suppress speckle noise in each SAR image. It is indicated that multitemporal speckle filter would result in smaller noise level while preserving spatial patterns (Lee et al., 2009; Lavreniuk et al., 2017). Multitemporal speckle filter applies a weighted average across all images in a time series data. The last step was conversion to decibel to warrant comparable information to previously published values.

3.2 Sigma Nought Backscatter Value Extraction (Field Level) and Descriptive Statistics

Backscatter temporal data analysis was based on field level. Extraction points were based on the centroid of each field, which account for 4743 points. We used ArcGIS to derive centroids and extract their coordinates, then collected sigma nought values on all Sentinel-1 imageries using SNAP. Sigma nought backscatter coefficient in decibel was plotted according to the days after transplanting. The Gaussian models fitting was employed on both polarizations to illustrate general trend of rice growth period.

3.3 Layers Manipulation and RGB False-Color Composite Construction

Varying backscatter values during rice growth highlighted the dynamics of rice fields. Using r.series toolbox in QGIS with GRASS 3.14, minimum and maximum values of each pixel were derived by aggregating operation for both VH and VV series (Figure 2). The difference between the minimum and maximum values for both polarizations was derived using raster calculator. As a result, each polarization encompassed three layers of maximum, minimum, and the difference between maximum and minimum values.

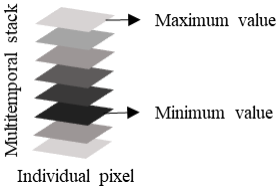

Figure 2 Illustration of pixel-wise r.series aggregation

False-color RGB composition was produced on each polarization to better visualize crop patterns using maximum, minimum, and difference layers. Different color patterns may vary depending on how layers were assigned to the RGB channels.

3.4 Threshold Determination and Rice Area Mapping

Rice area thresholds were generated using statistics and histogram toolbox in SNAP. Sample rice areas used to obtain threshold values were created according to the reference map. Several combinations of threshold were employed: a) maximum and minimum, b) maximum and difference, c) minimum and difference, d) maximum, minimum, and difference.

3.5 Accuracy Assessment

Accuracy assessment for classification was conducted using confusion matrix. Totalling 500 sampling points were employed using a stratified random scheme, distributed proportionally to sampling areas. Overall accuracy and its kappa statistics were calculated as a measure of the best performing classification scheme.

4. RESULTS AND DISCUSSION

4.1 Backscatter Behavior of Sentinel-1 Data

Studying backscatter temporal characteristics of rice field is vital for the development of future studies related to crop monitoring such as mapping and biophysical parameters estimation (Kuenzer and Knauer, 2013; Veloso et al., 2017). Figure 3 shows the behavior of backscatter coefficients of VH and VV. Phenological cycle of rice cultivars in the site takes up to 120 days (Yoshida, 1981). Twenty-day period of germination or seedling prior to transplanting is present in the figure to depict fluctuating sigma nought before transplanting. The reason is yet to be discovered and this warrants future investigation. Harvesting period is expected to be around 100th day after transplanting, and can be expanded up to 10 days depending on weather condition (raining means that the harvest will be postponed).

Backscatter started to decrease after seedling began and reached the lowest around -18 dB for VH and -10 dB for VV in transplanting date due to specular reflection from waterlogged rice fields. Thus, according to Choudhury et al. (2007), waterlogged period was crucial in identifying rice fields in time series radar data. In this set of data, there was an evidence of double-bounce or Bragg's scattering on both polarizations showed by the amplification or high signal responses at the beginning of rice cultivation as shown by Ouchi et al. (2006) Double-bounce effect was more prominent in VV polarization than VH. According to Twele et al. (2016) double-bounce effect indicated by strong signal return happened because of scattering at the water surface towards partially submerged trunks before returning to the sensor. This scattering mechanism preserved vertical linear polarization; hence, VV polarization showed higher signal responses than the one depicted in VH.

VH backscatter increased throughout rice growth period from the vegetative phase (~40 days after transplanting), generative phase (~70 days after), and ripening (~100 days after transplanting). Compared to VH, VV backscatter behavior varied greater and data possessed more fluctuation. This could happen because at C-band VV polarization is more sensitive towards any surface interactions involving less diffuse scattering condition. Meanwhile, VH polarization adapts to

slight volume scattering which was shown highly correlated with crop condition indicators (Ouchi et al., 2006; Twele et al., 2016; Vreugdenhil et al., 2018). Decreasing signal response starting before the 50th day after transplanting was probably linked with declining amount of tiller. According to Yoshida (1981), tiller number declines after its maximum at around 40th day after transplanting until tiller number equals to panicle number at maturity. During ripening phase, beginning at around 70th days after transplanting until harvesting period, backscatter signals were relatively stable. After harvesting, however, signal increased distinctively due to exposing bare soil.

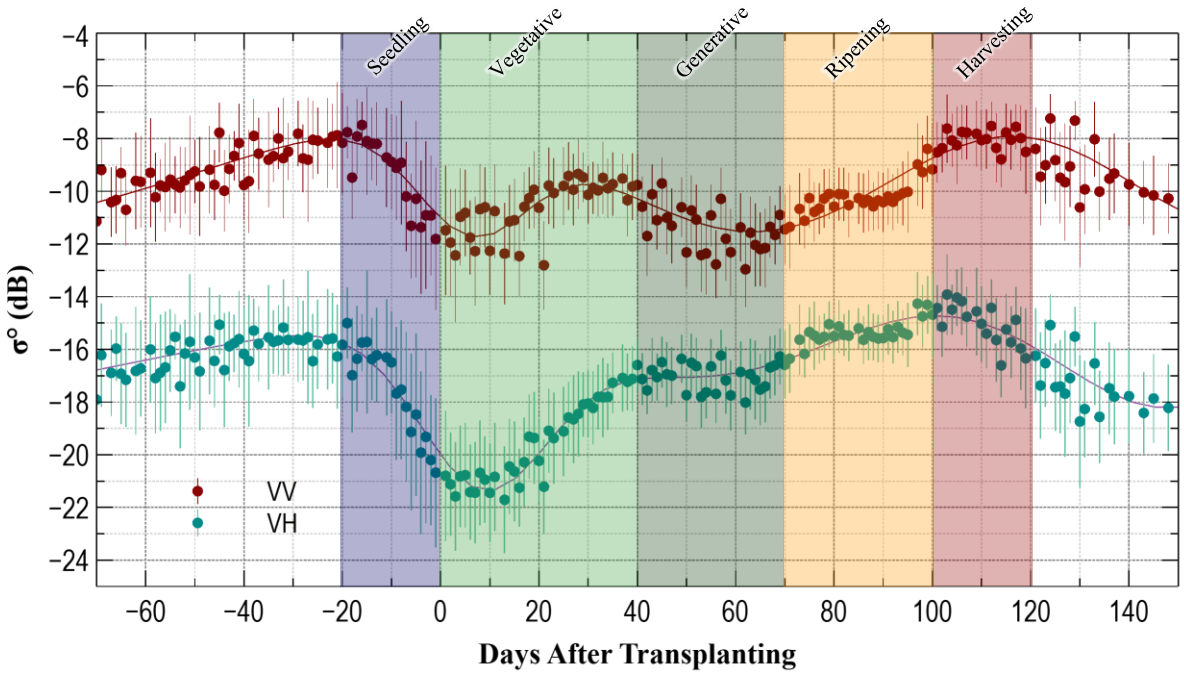

Figure 3 Varying backscatter coefficient with days after transplanting. Models shown in solid lines illustrate general trend of growth phase periods

4.2 Rice Area Detection and Mapping

Figure 4 visualizes each layer after r.series processing. Rice areas started to be visually discriminable, specifically on minimum and difference backscatter layers. On the minimum backscatter layer (Figure 4(b) and 4(e)), rice areas appear to be the darkest due to the lowest backscatter values that happened during flooding period. On the difference backscatter layer (Figure 4(c) and 4(f)), rice areas show up lighter due to a greater difference between high and low backscatter values throughout rice cultivation period. In order to improve visual separability, these layers were then assigned into RGB channels.

Figure 5 shows the RGB composite (red: maximum backscatter, green: minimum backscatter, blue: difference backscatter). On rice fields, the maximum backscatter layer represents harvesting period or bare soil, meanwhile minimum backscatter values indicate flooding period. The difference between the maximum and minimum backscatter coefficients which was assigned to the blue channel characterizes irrigated rice cultivation area as elaborated in the previous section. In this case, bluish areas in RGB composite correspond well to rice areas in both polarizations. RGB composite of VH polarization depicts a better impression in segregating rice areas in term of contrast, meanwhile in the case of VV polarization, less sensitivity towards difference of harvesting period or bare soil and flooding period is demonstrated.

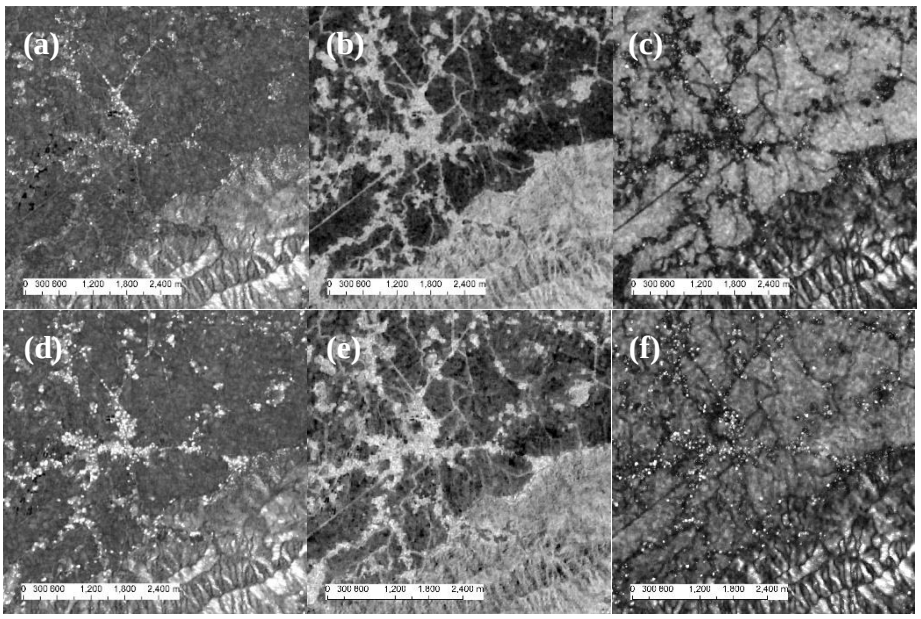

Figure 4 Pixel-wise calculation of maximum (a), minimum (b), and difference (c) on VH polarization and maximum (d), minimum (e), and difference (f) on VV polarization

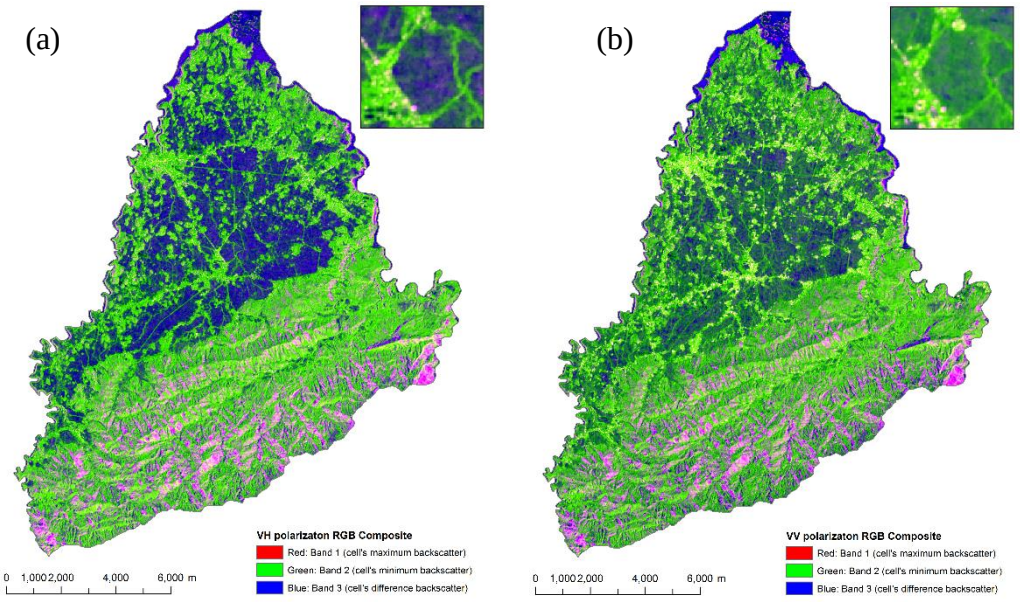

Figure 5 RGB false-color composite of VH polarization (a) and VV polarization (b)

Thresholding of backscattering coefficient to distinguish flood and non-flood areas, including rice fields, was successfully performed to the SAR data in various frequencies (Henry et al., 2006; Martinis et al., 2015; Ohki et al., 2019; Wakabayashi et al., 2019). In this research, we adopted this method to separate rice areas using several layer threshold combinations in search for the best performing one. In order to determine the threshold, sigma nought values from rice areas were retrieved based on several shapes guided by reference data. Figure 6 shows histograms of VV and VH sigma nought backscattering for each layer, while Table 2 presents threshold values using the 95th percentile (p95).

Thresholds presented in Table 2 applied to both VH and VV sigma nought images containing layers of maximum, minimum, and their difference. Several combinations were employed in

search for the best performing one in term of overall accuracy. The accuracy of rice and non-rice binary images was then be assessed by using confusion matrix in comparison with the reference map. Table 3 shows the accuracy assessment of each operation. Based on the result, combinations of maximum and minimum, and minimum and difference excelled on both polarizations. Generally, thresholding on sigma nought VH polarization image resulted in a better overall accuracy in comparison to the one presented by VV polarization. This study found that the best thresholding combination for separating rice from non-rice areas was maximum and minimum on sigma nought VH polarization. Figure 7 shows the rice map composed using the best-performing combination.

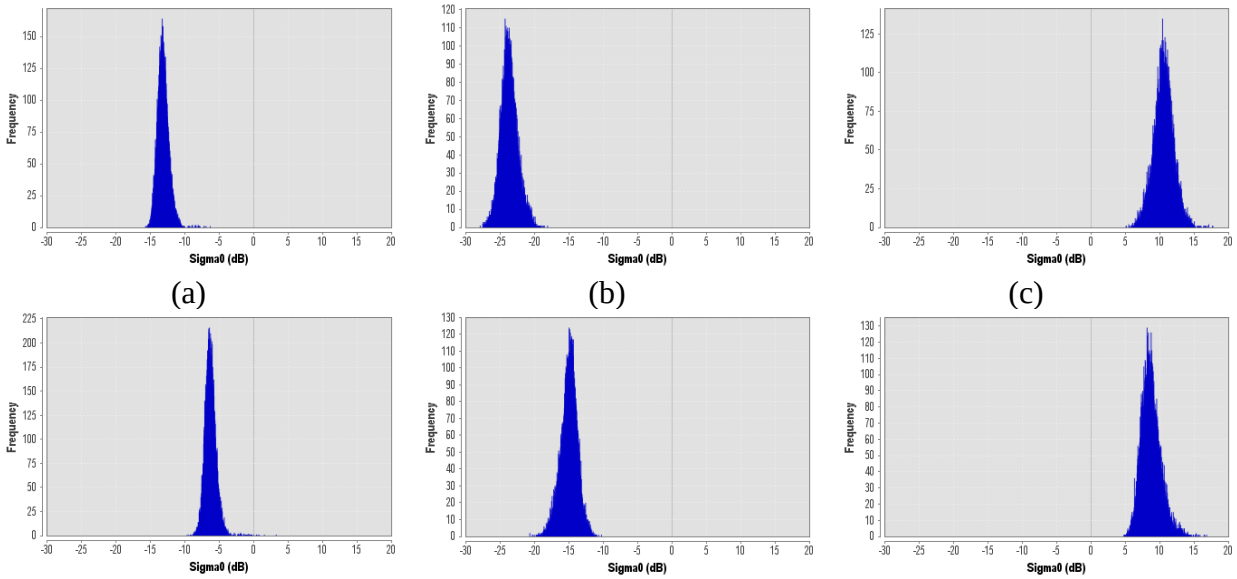

(a) (b) (c)

(d) (e) (f)

Figure 6 Histograms of VH maximum (a), minimum (b), and difference (c), and VV maximum (d), minimum (e), and difference (f) on rice fields

Table 2 Threshold values

Polarization	Layer	Threshold (p95)
VV	Maximum	-4.878
	Minimum	-13.107
	Difference	11.184
VH	Maximum	-11.753
	Minimum	-21.501
	Difference	12.906

Table 3 Accuracy of threshold combinations

Polarization	Threshold combination	Overall accuracy	Kappa
VV	Maximum and minimum	0.828	0.583
	Maximum and difference	0.794	0.569
	Minimum and difference	0.822	0.571
	Maximum, minimum, and difference	0.796	0.478
VH	Maximum and minimum	0.856	0.654
	Maximum and difference	0.778	0.555
	Minimum and difference	0.854	0.650
	Maximum, minimum, and difference	0.822	0.554

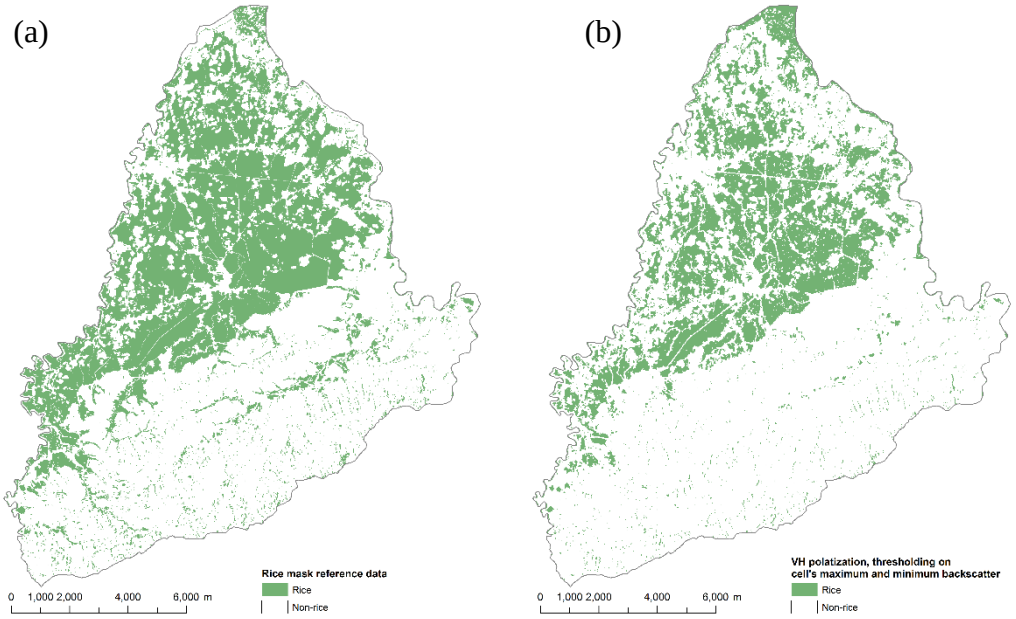

Figure 7 Rice reference map (a) and the one generated from Sentinel-1 VH polarization thresholding on maximum and minimum sigma nought values (b)

5. CONCLUSION

In this article, Sentinel-1 SAR data were shown invaluable to map irrigated rice areas using a computationally inexpensive yet fairly accurate method. Temporal behavior of SAR backscattering coefficient was discovered to be valuable information to differentiate rice area from others. Using layer manipulation and RGB false-color composite, visual separability of rice area could be comprehended. Thresholding on backscattering coefficient (Henry et al., 2006; Martinis et al., 2015; Ohki et al., 2019; Wakabayashi et al., 2019) was adapted to separate rice areas using threshold combinations in search for the best performing one. Except in a few cases, most time series combination contributed well to the discrimination with suitable accuracy (over 80%); hence, they open possibility for operational applications.

6. REFERENCES

Badan Pusat Statistik, 2018. 2018 Harvested Area and Rice Production in Indonesia. BPS-RI, Jakarta.

Badan Pusat Statistika, 2019. 2019 Harvested Area and Rice Production in Indonesia. BPS-RI, Jakarta.

Choudhury, I., Parihar, J.S. and Chakraborty, M., 2007. Estimation of rice growth parameter and crop phenology with conjunctive use of Radarsat and ENVISAT. In: Proc. 'Envisat Symposium 2007', Montreux, Switzerland.

Clauss, K., Ottinger, M. and Kuenzer, C., 2018. Mapping rice areas with Sentinel-1 time series and superpixel segmentation". International Journal of Remote Sensing, 39 (5), pp. 1399–1420.

Henry, J.B., Chastanet, P., Fellah, K. and Desnos, Y.L., 2006. Envisat multi-polarized ASAR data for flood mapping. International Journal of Remote Sensing, 27 (10), pp. 1921–1929.

Kuenzer, C., and Knauer, K., 2013. Remote sensing of rice crop areas. International Journal of Remote Sensing, 34 (6), pp. 2101–2139.

Lavreniuk, M., Kussul, N., Meretlsky, M., Lukin, M., 2017. Impact of SAR data filtering on crop

classification accuracy. In: 2017 IEEE First Ukraine Conference on Electrical and Computer Engineering (UKRCON), Kiev, 2017, pp. 912–917.
Lee, J.S., Wen, J.H., Ainsworth, T.L., Chen, K.S., Chen, A.J., 2009. Improved sigma filter for speckle filtering of SAR imagery. In: IEEE Transactions on Geoscience and Remote Sensing, 47 (1), pp. 202–213.
Martinis, S., Kersten, J., and Twele, A., 2015. A fully automated TerraSAR-X based flood service. ISPRS Journal of Photogrammetry and Remote Sensing, 104, pp. 203–212.
Munibah, K., Yudarwati, R., Wahyunie, E.D., and Wijaya, H., 2016. Protection of paddy field and recommendation of regional planning in Cianjur Regency, West Java, Indonesia. In: IOP Conference Series: Earth and Environmental Science, 47.
Ohki, M., Watanabe, M., Natsuaki, R., Motohka, T., Nagai, H., Tadono, T., Suzuki, S., et al., 2019. Flood area detection using ALOS-2 PALSAR-2 data for the 2015 heavy rainfall disaster in the Kanto and Tohoku area, Japan. In: IGARSS 2018 - 2018 IEEE International Geoscience and Remote Sensing Symposium, Valencia, 2018, pp. 8777–8780.
Ouchi, K., Wang, H., Ishitsuka, N., Saito, G., and Mohri, K., 2006. On the Bragg scattering observed in L-band synthetic aperture radar images of flooded rice fields. IEICE Transactions on Communications, E89-B (8), pp. 2218–2225.
Panuju, D.R., Mizuno, K., and Trisasongko, B.H., 2013. The dynamics of rice production in Indonesia 1961–2009. Journal of the Saudi Society of Agricultural Sciences. 12 (1), pp. 27–37.
Pulvirenti, L., Pierdicca, N., Squiccarino, G., Boni, G., Chini, M., Benedetto, C., 2016. Polarimetric SAR data for improving flood mapping: An investigation over rice flooded fields. In: 2016 IEEE International Geoscience and Remote Sensing Symposium (IGARSS), Beijing, 2016, pp. 7589–7592.
Refice, A., Capolongo, D., Pasquariello, G., Daaddabbo, A., Bovenga, F., Nutricato, R., Lovergine, F.P., et al., 2014. SAR and InSAR for flood monitoring: Examples with COSMO-SkyMed data. In: IEEE Journal of Selected Topics in Applied Earth Observations and Remote Sensing, 7 (7), pp. 2711–2722
Stroppiana, D., Boschetti, M., Azar, R., Barbieri, M., Collivignarelli, F., Gatti, L., Fontanelli, G., et al., 2019. In-season early mapping of rice area and flooding dynamics from optical and SAR satellite data. European Journal of Remote Sensing, 52 (1), pp. 206–220.
Trisasongko, B.H., 2017. Mapping stand age of rubber plantation using ALOS-2 polarimetric SAR data. European Journal of Remote Sensing, 50 (1), pp. 64–76.
Twele, A., Cao, W., Plank, S., and Martinis, S., 2016. Sentinel-1-based flood mapping: a fully automated processing chain. International Journal of Remote Sensing. 37 (13), pp. 2990–3004.
Veloso, A., Mermoz, S., Bouvet, A., Toan, L.T., Planells, M., Dejoux, J.F., and Ceschia, E., 2017. Understanding the temporal behavior of crops using Sentinel-1 and Sentinel-2-like data for agricultural applications. Remote Sensing of Environment. 199, pp. 415–426.
Vreugdenhil, M., Wagner, W., Bauer-Marschallinger, B., Pfeil, I., Teubner, I., Rüdiger, C., and Strauss, P, 2018. Sensitivity of Sentinel-1 backscatter to vegetation dynamics: An Austrian case study. Remote Sensing, 10 (9).
Wakabayashi, H., Motohashi, K., Kitagami, T., Tjahjono, B., Dewayani, S., Hidayat, D., and Hongo, C, 2019. Flooded area extraction of rice paddy field in Indonesia using Sentinel-1 SAR data. In: ISPRS - International Archives of the Photogrammetry, Remote Sensing and Spatial Information Sciences, Volume XLII-3/W7, 2019, pp.73–76.
Wiesmann, A., Wegmüller, U., Honikel, M., Strozzi, T., and Werner, C.L., 2001. Potential and methodology of satellite based SAR for hazard mapping. In: IEEE 2001 International Geoscience and Remote Sensing Symposium, Sydney, NSW, Australia, 2001, pp. 3262–3264.
Yoshida, S., 1981. Fundamentals of Rice Crop Science. The International Rice Research Institute, Los Banos.